

CHAPTER ONE

SUPERCONDUCTIVITY

In this chapter the phenomenon of superconductivity is introduced and some elementary theory presented. The practical applications and physical properties of high temperature superconducting materials are then examined in some detail, with a particular emphasis on the effect of grain boundaries on the electromagnetic properties.

1.1 Basic Phenomena

From 1908 H. Kamerlingh Onnes, having successfully liquefied helium, was able to measure the electrical resistance of metals at very low temperatures. The startling discovery made in 1911 was that as the temperature of a sample of Hg was reduced, the resistance did not fall continuously as expected, but instead at around 4.2 K dropped suddenly to zero over a range of a few hundredths of a degree [1]. This phenomenon was termed superconductivity and was found to occur for other elements such as Pb, Sn and Al at critical temperatures between 4-10 K. The fact that this is a real disappearance of the resistivity, rather than just a decrease below that measurable using a standard voltmeter, was confirmed by studying the persistence of circulating currents in a superconducting loop.

Another important property of superconductors was discovered in 1933 by Meissner & Ochsenfeld [2]. One would expect, due to the perfect conductivity, that magnetic flux should be excluded from entering a superconductor, but also it was found that flux was expelled from the material as it was cooled through its transition temperature. This phenomenon is termed the 'Meissner effect'. The expulsion of the magnetic field requires the flow of circulating 'screening currents' and hence the existence of the Meissner effect necessitates that the resistance must be zero. This 'perfect diamagnetism' demonstrates that superconductivity is a true thermodynamic state and that in moving from the normal to the superconducting state, a material undergoes a thermodynamic phase transition. In order for

this to happen, the overall free energy must be lower in the superconducting state than in the normal state and this energy difference, which depends on the temperature, is known as the condensation energy. When a magnetic field is applied to a material in the superconducting state, energy is required to prevent it from penetrating. If that is larger than the condensation energy, the material will lower its overall free energy by returning to its normal state. Thus there is a critical magnetic flux density, B_c , which is a function of temperature :

$$f_n(T) - f_s(T) = \frac{B_c^2(T)}{2\mu_0} \quad (1.1)$$

where f_n and f_s are the Helmholtz free energies of the normal and superconducting states respectively and μ_0 is the permeability of free space.

In addition to the requirement that the temperature and magnetic field must be below some value, there is also a limit on the current density in a superconducting material. Hence the three critical values T_c , H_c and J_c , which are all interdependent are shown in figure 1.1, and a material will only remain in the superconducting state within the volume shaded.

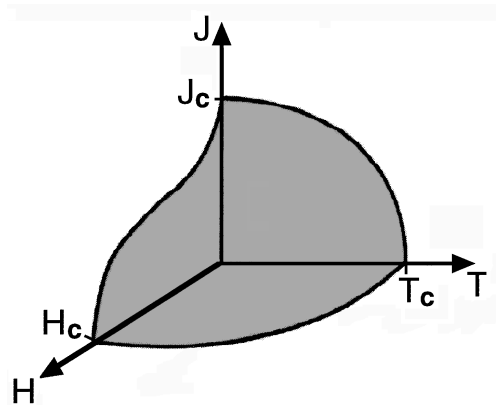


Figure 1.1 Schematic of the regions of current density, magnetic field and temperature within which a material remains superconducting.

1.2 Elementary Phenomenological Theories

1.2.1 The London theory

In 1935, F. and H. London proposed the following equations to govern the microscopic electric field, \mathbf{E} , and magnetic field, \mathbf{h} , in superconductors [3].

$$\mathbf{E} = \frac{\partial}{\partial t} (\Lambda \mathbf{J}_s) \quad (1.2)$$

$$\mathbf{h} = -\nabla \times (\Lambda \mathbf{J}_s) \quad (1.3)$$

$$\text{where} \quad \Lambda = \mu_0 \lambda_L^2 = m_e / n_s e^2 \quad (1.4)$$

for a number density of superconducting electrons n_s , where \mathbf{J}_s is the supercurrent density and m_e the electronic mass.

Equation (1.2) is an acceleration equation which describes the perfect electrical conductivity.

Equation (1.3) may be combined with the Maxwell equation $\nabla \times \mathbf{h} = \mu_0 \mathbf{J}$ to give

$$\nabla^2 \mathbf{h} = \mathbf{h} / \lambda_L^2 \quad (1.5)$$

the solution of which is the exponentially decaying $h = h_0 \exp(-x/\lambda_L)$, i.e. the magnetic field is screened from the interior of a sample within a distance λ_L , known as the ‘penetration depth’.

1.2.2 The Ginzburg-Landau theory

In 1950, Ginzburg and Landau [4] proposed a theory based on Landau’s general theory of 2nd order phase transitions. The superconducting electrons were described by a complex wavefunction, ψ , such that $n_s = |\psi|^2$. By expanding the expression for the free energy, a differential equation may be derived for ψ :

$$\frac{1}{2m} (-i\hbar \nabla + 2e\mathbf{A})^2 \psi + (\alpha + \beta \psi \psi^*) \psi = 0 \quad (1.6)$$

The supercurrent density is given by :

$$\mathbf{J}_s = \frac{ie\hbar}{m}(\psi^* \nabla \psi - \psi \nabla \psi^*) - \frac{4e^2}{m} \mathbf{A} \psi \psi^* \quad (1.7)$$

where \mathbf{A} is the magnetic vector potential such that $\mathbf{B} = \text{curl } \mathbf{A}$.

The Ginzburg-Landau equations lead to two characteristic lengths, the G-L penetration depth, λ_{GL} ,

$$\lambda_{\text{GL}} = \sqrt{(m\beta / 4\mu_0 e^2 |\alpha|)} \quad (1.8)$$

and the coherence length, ξ

$$\xi = \sqrt{(\hbar^2 / 2m |\alpha|)} \quad (1.9)$$

where α is proportional to $(T - T_c)$ and β is approximately independent of T .

The penetration depth is, like the London penetration depth, the characteristic length for the decay of the magnetic field in a superconductor. The coherence length may be described as the length scale over which the order parameter varies.

As both λ_{GL} and ξ are inversely related to α , they are dependent on temperature and both diverge as T approaches T_c . However, the ratio of the parameters,

$$\kappa = \lambda_{\text{GL}} / \xi \quad (1.10)$$

which is known as the Ginzburg-Landau parameter, does not depend on α and is therefore approximately independent of temperature.

1.2.3 Type I and type II superconductors

In 1957, Abrikosov [5] showed that solutions of the Ginzburg-Landau equations fall into two distinct categories. For $\kappa < 1/\sqrt{2}$, the surface energy of the interface between the normal and

superconducting phases is positive. Thus the behaviour noted by Meissner is observed, whereby flux is completely excluded from the material below T_c . This behaviour is known as Type I. For $\kappa > 1/\sqrt{2}$ however, the surface energy of a normal/superconducting interface is negative and it will therefore be energetically favourable for flux to exist within the superconducting material – so called Type II behaviour. In order to achieve the minimum energy state, the area of the boundary between superconducting and normal material is maximised and so the normal regions are subdivided until a quantum limit is reached. Thus for Type II materials, instead of there being an abrupt breakdown of superconductivity at B_c , there is a lower critical field, B_{c1} , at which flux begins to penetrate, but total penetration only occurs at an upper critical field, B_{c2} , which may be much higher. When in the “mixed state” between B_{c1} and B_{c2} , the superconductor contains individual flux quanta which are supported by circulating supercurrents. Hence the remainder of the material remains superconducting.

1.3 Power Applications of High Temperature Superconductors

The motivation for the development of superconducting coated conductors lies in the many applications for which they could provide superior performance to the materials which are currently in use. As superconductors are more efficient than conventional materials, significant energy savings in the power generation and distribution industry may be made, with obvious economic and environmental gains. Also superconducting materials are often necessary for applications which require high current densities, not obtainable using normal metals. The advantages of high T_c materials over low T_c conductors such as Nb_3Sn and $NbTi$ include the higher upper critical field, B_{c2} , and higher critical current density, J_c , as well as the fact that they can be used at higher temperatures leading to potential savings in cryogen costs.

1.3.1 Power generation and storage

One potential application of HTS in the power industry is in electrical generators. In addition to the improved efficiency that the use of superconducting rotors would offer, a reduction in size and weight of such a unit is an attractive prospect. The majority of projects to date have

used LTS materials [6] with the most ambitious project undertaken being the Super-GM project in Japan involving the development of a 100 MVA unit [7]. However the prospects for more widespread use of HTS materials in superconducting generators are rather poor partly due to the fact that components presently in use in the electricity generation industry are extremely reliable, but also because of difficulties in reducing AC losses in HTS tapes [8].

Potential applications in energy storage are superconducting magnetic energy storage (SMES) and superconducting flywheels. SMES works by storing energy in a magnetic field produced by coils which carry a large superconducting d.c. current with no ohmic losses. Such a machine would be useful for meeting diurnal variations in electricity demand, or as an emergency power source [9]. There are several small units in operation which store around 1 MJ [7], though these use low T_c materials such as NbTi and significant improvements in the quality of HTS materials are required in order for them to become competitive [8]. Superconducting flywheels use the principle that a superconducting stator may be suspended in mid-air and thus spin with incredibly low friction. Rotational kinetic energy can thus be stored and used to provide power for short periods of time, during temporary faults [10]. Such machines may presently be manufactured using YBCO, but to be of practical use on a large scale, losses will have to be reduced from those presently achievable [11].

1.3.2 Electricity transmission and distribution

Potential applications in the electricity distribution industry are more promising. One use of a superconducting wire is to produce a transmission cable – in urban areas, where large amounts of power must be transmitted by underground cables, high current density is important and thus superconducting wires are an attractive proposition. In the US, approximately 100 miles of existing underground cables are replaced each year, representing a market of around \$200 million. Since the discovery of HTS materials, several companies have produced cables using BSCCO tapes [7, 12]. One project has recently produced a 30 m long, 3 phase HTS cable which replaced a conventional cable in use at the Southwire

company HQ [13]. The cable carries 1250 A at 12.4 kV and has operated continuously for 3000 hours [11].

There is also interest in the development of transformers, where superconducting materials would have several advantages over those using conventional materials. The main benefit is that losses in the windings are significantly reduced, allowing a reduction in the number of ampere turns used. This leads to a significant reduction in the amount of magnetic flux and hence fewer iron core losses. The main practical advantage is a reduction in the physical size and weight of the coils. Calculations based on an 850 MVA unit [14] have demonstrated that a transformer using HTS materials at 77 K would lead to losses being reduced by a factor of 7 and facilitate a reduction in weight by a factor of 5. A small scale (630 kVA) transformer was manufactured in 1997 using BSCCO [7] and installed in a substation of the Geneva utility company. At present, a 5-10 MVA development, also using BSCCO, aims to supply power to the Waukesha Electric Systems plant in Wisconsin.

Another application of superconducting materials is the fault current limiter, which uses the resistive transition to reduce the fault current in an electrical circuit. Because the transition happens in less than 1 ms, it is possible to prevent damage to circuit components which can be caused by excess current in the time (around 50 ms) taken for conventional circuit breakers to trip. HTS materials are in principle suitable for use in FCLs although most 1st generation conductors are composites containing low resistivity metals (i.e. silver), which would compromise the limiting effect [15]. A prototype HTS FCL is being developed in China for testing in 2001 [12].

1.3.3 Magnet applications

There are a number of industrial applications based on the ability of superconductors to provide very high field magnets. One such application is in magnetic separation and filtration, which has been performed widely using conventional magnets for some time [16], for example in the enrichment of ferromagnetic iron ores. For small particles which are only

weakly ferromagnetic or paramagnetic, much larger fields (and field gradients) are needed for separation [17].

A high profile application of superconducting magnets is to facilitate high speed levitating trains, where the advantages include speed, safety and environmental benefits. A number of projects have been undertaken using conventional magnets such as the German Transrapid system, and test tracks which use LTS materials have also been successfully built, notably the Yamanashi line in Japan [8]. High field magnets are also of importance in research fields such as high energy physics. Particle detector magnets and accelerator beam guidance magnets are both ideally served by superconductors. Notable examples of LTS materials in use at present include the Large Hadron Collider at CERN and the TEVATRON in the US. Projects using HTS include the development of BSCCO for the ‘Very Large Hadron Collider’ [18]. A major market for superconducting materials is magnets for magnetic resonance imaging (MRI), primarily for medical diagnostics. As with most other applications, commercial superconducting systems are still based on NbTi. Whilst experimental systems have been built using HTS materials, the main problem is the high cost of BSCCO.

1.3.4 Summary

There are many potential applications of high T_c coated conductors, most of which have already been put into practice using LTS materials such as NbTi and Nb₃Sn. Where HTS materials have broken through, the only material presently available for use is BSCCO in which the relatively low critical current is a serious limitation. In order to be competitive with both conventional materials and low temperature superconductors on a major scale, the performance of HTS wires and tapes needs to be improved considerably over those which can be manufactured in long lengths at present. In addition the combined cost of materials and manufacture must be reduced to around \$10/kAm.

1.4 High Temperature Superconductors

1.4.1 Introduction

Until 1986, the record transition temperature for a superconductor was 23 K [19]. In that year, Bednorz and Muller [20] synthesised the compound La_2CuO_4 which remains superconducting up to 30 K, and soon afterwards other superconducting cuprate materials were discovered with even higher transition temperatures. $\text{YBa}_2\text{Cu}_3\text{O}_{7-\delta}$ (YBCO) has a T_c of 92 K [21], which is significant because it is greater than the boiling point of liquid nitrogen at atmospheric pressure. Bi-Sr-Ca-Cu-O, Tl-Ba-Ca-Cu-O [22] and Hg-Ba-Ca-Cu-O [23] compounds have higher critical temperatures as shown in table 1.1.

Table 1.1 Transition temperatures of some high T_c superconducting compounds [24-26]

Material	T_c (K)
$\text{YBa}_2\text{Cu}_3\text{O}_{7-\delta}$	92
$\text{Bi}_2\text{Sr}_2\text{CaCu}_2\text{O}_8$	85
$\text{Bi}_2\text{Sr}_2\text{Ca}_2\text{Cu}_3\text{O}_{10}$	110
$\text{TlBa}_2\text{Ca}_2\text{Cu}_3\text{O}_9$	123
$\text{HgBa}_2\text{Ca}_2\text{Cu}_3\text{O}_8$	135

All these high temperature superconductors have highly anisotropic crystal structures, containing layered CuO_2 planes in which the superconducting charge carriers are thought to be localised.

1.4.2 YBCO

The unit cell of YBCO is based on a stack of three perovskite cells as shown in figure 1.2 and the lattice type is either tetragonal or orthorhombic, depending on the oxygen content. The central perovskite cell contains an Y atom, sandwiched between CuO_2 planes. Adjacent to the CuO_2 planes are layers of BaO_2 and at the top and bottom of the cell there are Cu-O chains which have variable oxygen content, dependent upon the overall oxygenation level of the material.

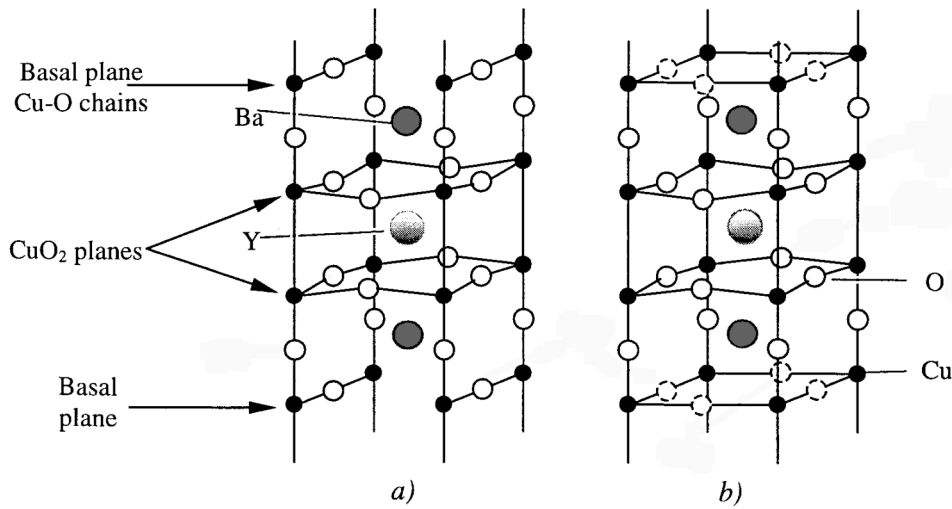


Figure 1.2 Unit cell of a) $YBa_2Cu_3O_7$ and b) $YBa_2Cu_3O_{7-\delta}$. The dashed circles indicate oxygen sites which are partially filled [27].

The HTS compounds can be described using a four number naming scheme, the numbers representing :

- 1) The number of insulating layers between CuO_2 planes (for YBCO, 1, the basal plane)
- 2) The number of spacing layers between blocks of CuO_2 planes (for YBCO, 2, the BaO_2 layers)
- 3) The number of separating layers within each block of CuO_2 planes (for YBCO, 1, the Y layer)
- 4) The number of CuO_2 layers in each block (for YBCO, 2)

Thus the crystal structure may be represented as in figure 1.3. Each square based pyramid has O atoms at its apices and a Cu atom at the centre of the base. The square Cu-O sheets have an O atom at each corner and a Cu atom at the centre. Note that in order to show two complete blocks of CuO_2 planes, the origin of figure 1.3 is shifted by $(0,0,\frac{1}{2})$ relative to the conventional cell shown in figure 1.2.

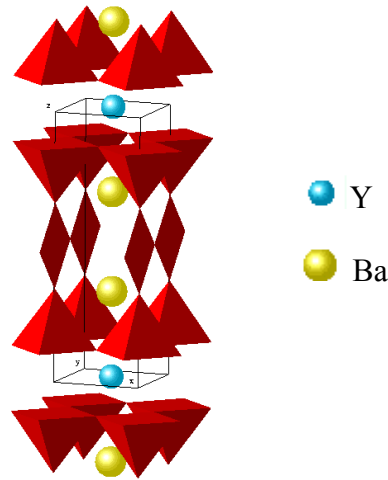


Figure 1.3 The crystal structure of YBCO. The pyramids have O atoms at the apices and Cu atoms at the centre of the base [28, 29].

The variation of the oxygen content in $\text{YBa}_2\text{Cu}_3\text{O}_{7-\delta}$ is extremely important in determining the superconducting properties. The effect of reducing the oxygen content below 7 atoms per unit cell is shown in figure 1.4. An optimum T_c of 93 K is obtained for $\delta=0.08$, but if more oxygen is removed from the structure, T_c falls rapidly and for $\delta>0.56$, $\text{YBa}_2\text{Cu}_3\text{O}_{7-\delta}$ is not superconducting. Also important for the superconducting properties of YBCO is the existence of chains of Cu-O atoms, which have metal-like electrical properties and reduce the anisotropy of the superconductor.

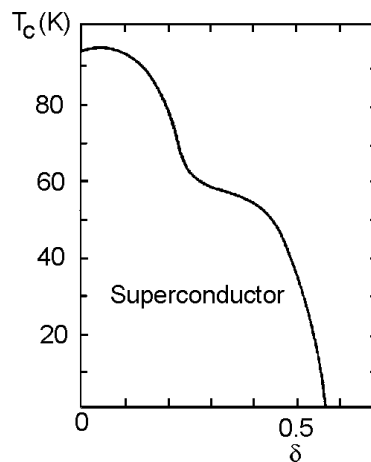


Figure 1.4 The effect of oxygen content on the T_c of $\text{YBa}_2\text{Cu}_3\text{O}_{7-\delta}$. Adapted from [27].

The variation of the unit cell parameters of YBCO with oxygen content is shown in figure 1.5, which demonstrates the tetragonal-orthorhombic transition at around $\delta=0.6$. Although the superconducting phase of YBCO is orthorhombic, in practice it is not possible to distinguish a and b directions in a macroscopic sample due to twinning on a fine scale.

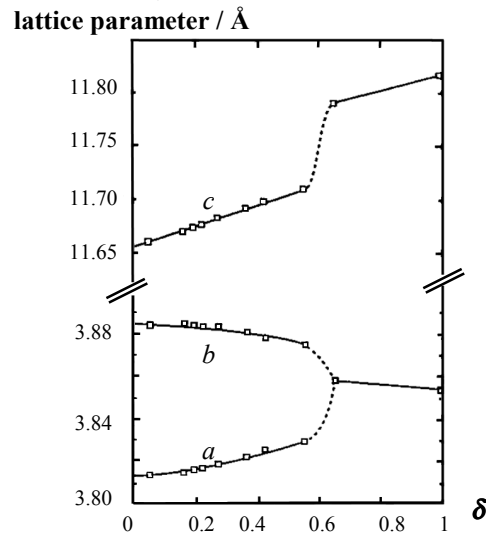


Figure 1.5 The unit cell parameters of YBCO as a function of the oxygen content. Adapted from [30].

The large anisotropy of the crystal structure has consequences for the physical properties as the effective mass of the electrons moving in the a-b plane, m_{ab} , is different from that in the c direction, m_c . This difference is characterised by an anisotropy parameter, γ , such that $\gamma^2 = m_c/m_{ab}$. The anisotropy parameter is a measure of the ratio of the coherence length and the penetration depth in the a-b plane and c-direction. For YBCO, γ is approximately 5-7 as demonstrated by the values shown in table 1.2.

Table 1.2 Anisotropy of ξ and λ in YBCO ($T=0$ K) [25, 31].

	Coherence length, ξ (nm)	Penetration depth, λ (nm)
a-b plane	2	140
c direction	0.3	900

The large Ginzburg-Landau parameter ($\kappa=\lambda/\xi$) means that YBCO is very strongly type II. The lower critical field B_{c1} is around 10 mT at 77 K compared with an upper critical field B_{c2} of over 800 T for field in the c-direction at $T=0$ K [31].

1.4.3 BSCCO

The superconducting compounds of Bi-Sr-Ca-Cu-O are based on $\text{Bi}_2\text{Sr}_2\text{Ca}_n\text{Cu}_{n+1}\text{O}_{6+2n}$, where n is an integer. The structures of the $n=1$ and $n=2$ compounds, generally known as Bi-2212 and Bi-2223 are shown in figure 1.6.

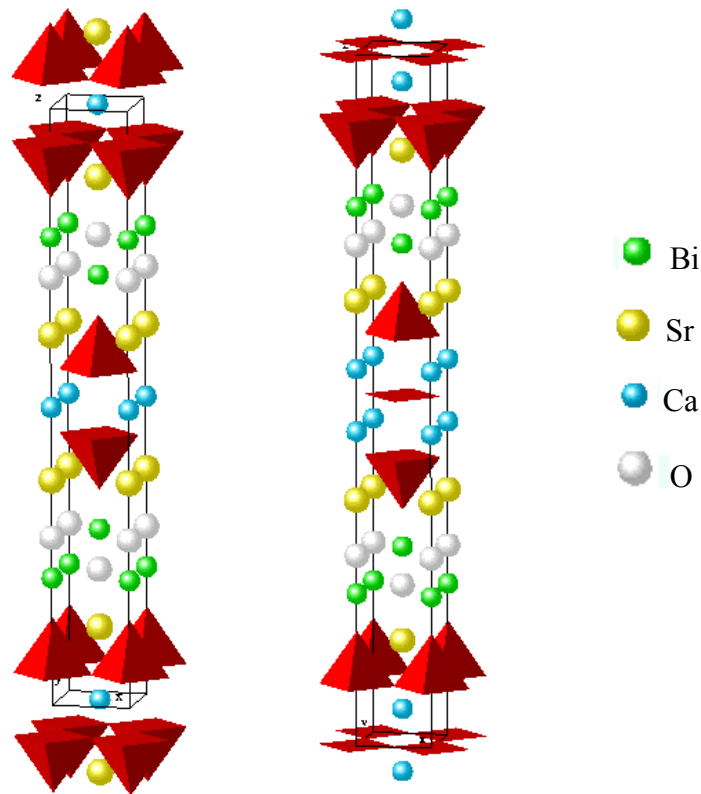


Figure 1.6 The crystal structures of Bi-2212 and Bi-2223 [28, 29].

BSCCO-2223 is an extremely anisotropic material, the value of γ being at least an order of magnitude greater than that in YBCO. Values of the coherence length and penetration depth are difficult to measure accurately and there is significant variation in the data reported in the literature, though some estimates are given in table 1.3.

Table 1.3 Anisotropy of ξ and λ in BSCCO ($T=0$ K) [30, 32]

		Coherence length, ξ (nm)	Penetration depth, λ (nm)
BSCCO-2212	a-b	3	300
BSCCO-2212	c	0.4	500
BSCCO-2223	a-b	2.0	
BSCCO-2223	c	0.04	

1.4.4 Thallium and mercury based compounds

There are several families of superconducting materials which incorporate Tl. The $\text{Tl}_2\text{Ba}_2\text{Ca}_n\text{Cu}_{n+1}\text{O}_{2n+6}$ system is analogous to the Bi based material with equivalent crystal structures and similar inter-layer spacings. In addition, the ‘single Tl-O layer’ $\text{TlBa}_2\text{Ca}_{n-1}\text{Cu}_n\text{O}_{2n+3}$ and $\text{TlSr}_2\text{Ca}_{n-1}\text{Cu}_n\text{O}_{2n+3}$ are superconducting. The $n=1$ and $n=2$ structures are shown in figure 1.7.

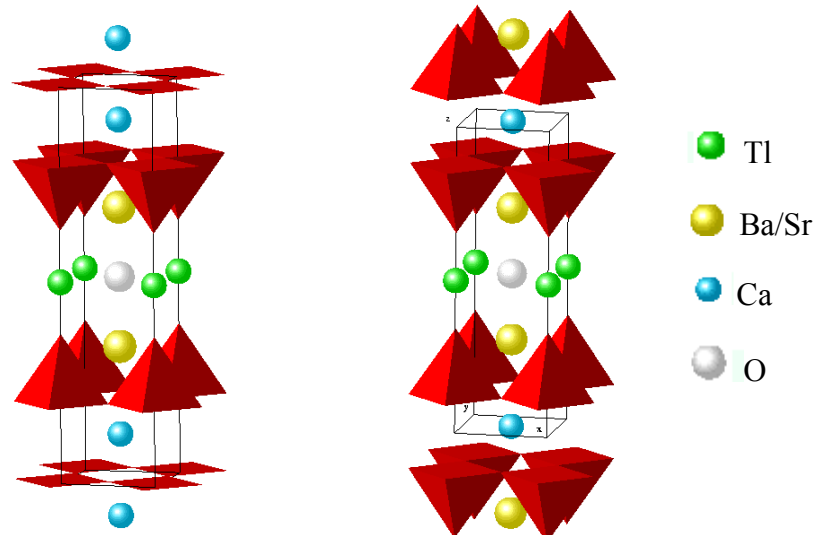


Figure 1.7 Crystal structures of 1212 and 1223 [28, 29].

The TSCCO compounds can be difficult to synthesise unless the Tl is partially substituted by Pb or Bi and the critical temperatures are generally lower than those of TBCCO, although they may be increased to 100 K with appropriate doping [33]. The superconducting properties

of the Tl compounds are less sensitive to oxygen stoichiometry than YBCO [34] and in terms of anisotropy, they lie somewhere between YBCO and BSCCO.

Of all the high T_c materials fabricated to date, those with the highest transition temperatures are the Hg based compounds. $\text{HgBa}_2\text{Ca}_2\text{Cu}_3\text{O}_8$, which has the same crystal structure as Tl-1223, has a T_c of 135 K, which can be increased by application of pressure. Due to the fact that the Hg compounds are closely related to the Tl materials in terms of their crystal structures, they have similar superconducting properties.

1.4.5 Summary

The high T_c materials have highly anisotropic crystal structures which leads to anisotropic physical properties. This anisotropy is related to the spacing between the superconducting Cu-O planes. An additional factor, which makes YBCO much less anisotropic than the other materials is the presence of Cu-O chains between the cuprate planes.

Table 1.4 Lattice parameters of common high T_c materials [28, 32].

	a / Å	b / Å	c / Å
YBCO	3.82	3.89	11.7
Bi-2212	3.81	3.81	30.6
Bi-2223	3.83	3.83	37.0
Tl-1212	3.86	3.85	12.8
Tl-1223	3.84	3.84	15.9
Hg-1223	3.86	3.86	17.7

1.5 Flux Vortices, Pinning and Critical Currents in Type II Superconductors

HTS conductors in use in applications such as those outlined in section 1.3 will invariably be in the mixed state, between B_{c1} and B_{c2} . Thus in order to understand the superconducting

properties of such materials it is important to examine the behaviour of magnetic field within such materials.

1.5.1 Flux vortices

Magnetic flux penetrates into a type II superconductor in the form of flux lines or vortices. The vortex, a cylinder with a core of radius ξ contains a region of suppressed order parameter which decreases to zero at the vortex centre, whilst the local magnetic field rises to a maximum as shown in figure 1.8.

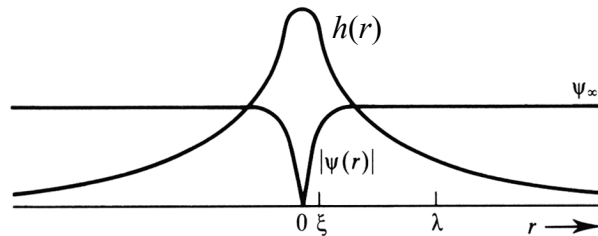


Figure 1.8 Variation of order parameter and local flux density for a single flux vortex. From reference [35].

Abrikosov [5] predicted by solving the Ginzburg-Landau equations that vortices inside a type II material should form a regular lattice. The arrangement with the lowest free energy turns out to be a triangular lattice, confirmed experimentally by Essmann and Trauble [36], who observed the flux lines in an electron microscope.

The large anisotropy of HTS materials causes changes to the structure of flux vortices. The differences in values of the coherence length and penetration depth in the a-b and c directions means that the form of a vortex depends on its direction relative to the crystallographic axes. The vortex core will have radius ξ_{ab} in the a and b directions and radius ξ_c in the c direction, as shown in figure 1.9.

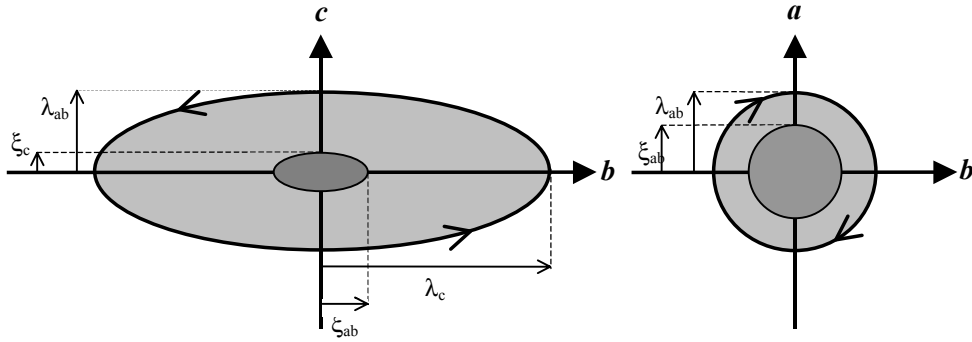


Figure 1.9 Schematic of vortices along the a axis and c axis of a uniaxially anisotropic type II superconductor. The inner shaded region represents the vortex core and the outer perimeter is a line of constant field. Adapted from reference [35].

The approximate ratios of the dimensions in figure 1.9 for YBCO are $\xi_{ab} \approx 5\xi_c$, $\lambda_c \approx 5\lambda_{ab}$ and $\lambda_{ab} \approx 100\xi_c$ [31].

In addition to this anisotropy, the layered nature of the high temperature superconductors is also important to the vortex structure. If the coherence length is significantly larger than the interplanar lattice spacing, the homogeneous 3-dimensional description holds. This is the case close to T_c (as ξ diverges at $T=T_c$), but as the temperature is lowered, ξ_c becomes smaller than the plane spacing. In this situation, the copper-oxygen planes are no longer well coupled and the best description of the material is as a stack of superconducting planes. The description of the flux vortices must be modified to take into account the fact that they are localised within the planes. Thus the result is an array of ‘pancakes’ [37], confined to the CuO_2 planes and only weakly coupled to their neighbours. If the magnetic field is in the c direction, the flux pancakes form a simple stack, but for field parallel to the a - b plane, vortices may form between the superconducting planes. These vortices, known as Josephson vortices, have no normal core and thus do not strongly suppress the order parameter in the adjacent superconducting planes. For fields at intermediate angles, the vortex can be described as a combination of pancake vortices in the c -direction (confined within CuO_2 planes) connected by Josephson vortices in the a - b plane as shown in figure 1.10.

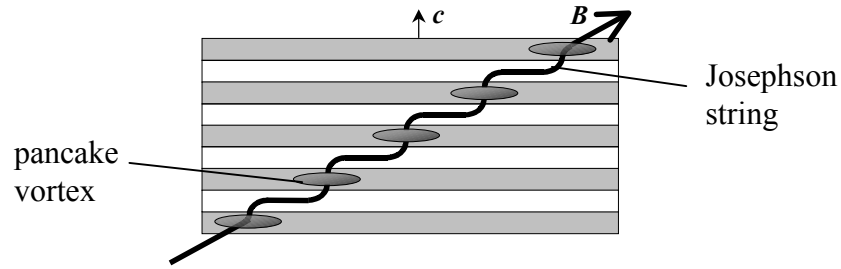


Figure 1.10 A flux vortex in an anisotropic layered superconductor [38].

1.5.2 Flux flow

In the presence of a macroscopic transport current \mathbf{J} , a flux vortex is subject to a Lorentz force per unit length $\mathbf{f}_L = \Phi_0 \mathbf{J} \times \mathbf{n}$, where \mathbf{J} is the current density, \mathbf{n} is a unit vector along the flux line and Φ_0 is the flux quantum. Averaging over a number of vortices gives the Lorentz force density,

$$\mathbf{F}_L = \mathbf{J} \times \mathbf{B} \quad (1.11)$$

This force tends to move flux lines in a direction perpendicular to that of the current flow, inducing an electric field normal to both the movement and the field direction. The value of the electric field is given by

$$\mathbf{E} = \mathbf{B} \times \mathbf{v} \quad (1.12)$$

where \mathbf{v} is the velocity of the moving flux line.

A simple model of flux flow considers a viscous drag coefficient η , such that the viscous force per unit length on a vortex moving with velocity \mathbf{v} is $-\eta\mathbf{v}$. Then a simple force balance equation is

$$\Phi_0 \mathbf{J} = -\eta\mathbf{v} \quad (1.13)$$

and the flux flow resistivity, ρ_f , defined by $E = \rho_f J$ is given by

$$\rho_f = \frac{E}{J} = \frac{B\Phi_0}{\eta} \quad (1.14)$$

This flux flow resistivity is related approximately to the normal state resistivity, ρ_n , and the upper critical field, B_{c2} , by

$$\rho_f \approx \rho_n \frac{B}{B_{c2}} \quad (1.15)$$

1.5.3 Flux pinning

In order that dissipation by flux flow does not begin as soon as vortices enter a type II material, it is necessary that there is a force opposing the Lorentz force to ‘pin’ the vortices in place. Such vortex pinning sites are provided by defects in the superconductor which act as energetically favourable sites at which a flux line can reside. Pinning centres may be point defects such as vacancies, line defects such as dislocations or plane defects such as grain boundaries. The presence of such favourable sites for pinning creates an average pinning force for the flux line lattice, F_p , which opposes the Lorentz force. Hence there is a finite critical current density, J_c , as sketched in figure 1.11.

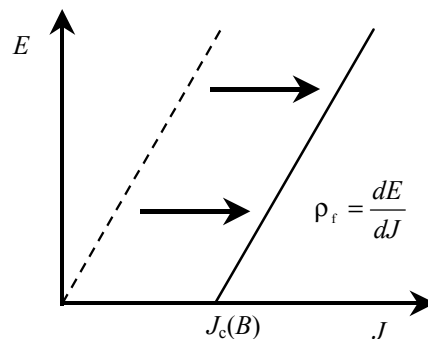


Figure 1.11 Schematic E - J characteristic for linear flux flow.

The degree of pinning varies dramatically amongst high T_c materials. In BSCCO and TBCCO, there are very few effective pinning sites and hence critical current values tend to be low. Bulk YBCO is slightly better, but J_c is still limited to around 10^4 - 10^5 Acm⁻² at 77 K. By far the best pinning is achieved in thin films, where J_c may be increased above 10^6 A cm⁻² by the incorporation of a high density of defects on a length scale of around 1 nm. An alternative method of increasing the pinning is to introduce artificial pinning sites, which may be achieved by irradiating a sample with fast neutrons.

1.5.4 Flux creep

Even whilst the average pinning force remains stronger than the Lorentz force and flux flow is prevented, there may still be dissipation caused by thermal fluctuations. One or more flux lines may jump from one pinned configuration to another, overcoming the energy barrier by thermal activation. In the absence of a current, the net movement of flux will be zero, but when a small current flows, it becomes more probable that any fluctuation will cause a flux line to move in the direction of the Lorentz force, and hence there is a net flux motion in that direction. As the current increases, the number of ‘forward’ jumps increases and the number of ‘backward’ jumps decreases, increasing the net movement of flux.

1.5.5 Critical currents in high temperature superconductors

In high T_c materials, thermal effects tend to dominate the early stages of dissipation due to the fact that the activation energy is smaller than for conventional type II materials and also because they are usually used at higher temperatures, hence the thermal energy is greater. This causes a significant curvature of the E - J characteristic around J_c . This is quantified by the ‘n-value’ of the transition, where $E=\rho J^n$. The flux flow regime is difficult to access experimentally as it only becomes dominant at high electric fields, though importantly it has been shown to be the mechanism of dissipation at grain boundaries [39], where the local electric field can be as high as 3 Vcm⁻¹.

In practical terms, there is a magnetic field which is more important for high T_c materials than the fields H_{c1} and H_{c2} . The irreversibility field, H_{irr} , is the field above which flux pinning becomes ineffective and moving flux lines cause dissipation. The irreversibility line, which describes the variation of H_{irr} with temperature is concave, unlike the upper and lower critical fields and its position depends not only on the level of pinning, but more importantly the degree of coupling between CuO_2 planes. Hence for poorly coupled materials such as BSCCO, the irreversibility line is much lower than for materials such as YBCO, as demonstrated by figure 1.12.

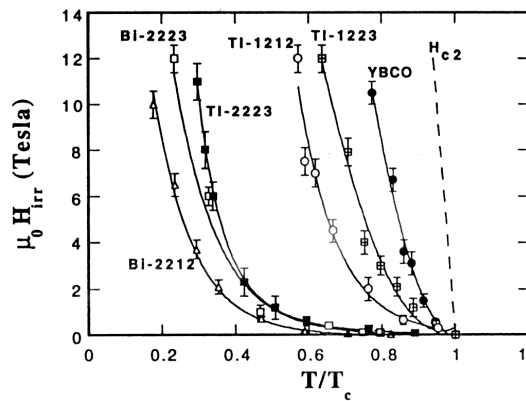


Figure 1.12 The position of the irreversibility line for various high T_c materials [30].

1.6 Grain Boundaries in High Temperature Superconductors

1.6.1 The relationship between critical current and boundary misorientation angle

The large difference between the critical currents achieved in textured materials and random polycrystals in early experiments on high T_c materials indicated that the grain boundaries are responsible for reducing $J_c^\#$. This was first demonstrated directly by Chaudhari et al. [40] who measured the critical current inside a grain and across a grain boundary in an YBCO film and found the inter-grain critical current to be more than an order of magnitude lower. The effect of the grain boundary misorientation angle was studied by Dimos et al. who

[#] In this thesis, J_c will represent a macroscopic critical current density, such as that measured in a large sample. Critical current densities on a microscopic scale, i.e. for an individual grain boundary, will be denoted by j_c .

fabricated thin films of YBCO on STO bicrystals [41]. They originally focussed on [001] tilt boundaries and found that the ratio of the grain boundary critical current to that of the grains fell as approximately θ^{-1} as shown in figure 1.13a). There is quite a significant spread in this data which may be caused by two factors. Firstly, the values that were measured for the intra-grain critical currents are very inconsistent, varying by up to a factor of 50 between samples. Within individual samples there is generally more consistency but j_c is still seen to vary by to a factor of 4 in different tracks on the 22.5° sample. It was to allow for this variation that the value of the boundary j_c was normalised relative to the average j_c measured in the grains. The misorientation angle which was plotted is that in the basal (a-b) plane, though due to difficulties in producing bicrystal substrates with perfectly aligned c-axes, the grain boundaries studied actually included out-of-plane misorientation components ranging from 2°-9°. If the data is plotted against the total misorientation angle, there is less scatter at low angles as shown in figure 1.13b) which indicates an exponential reduction of the critical current at low angles.

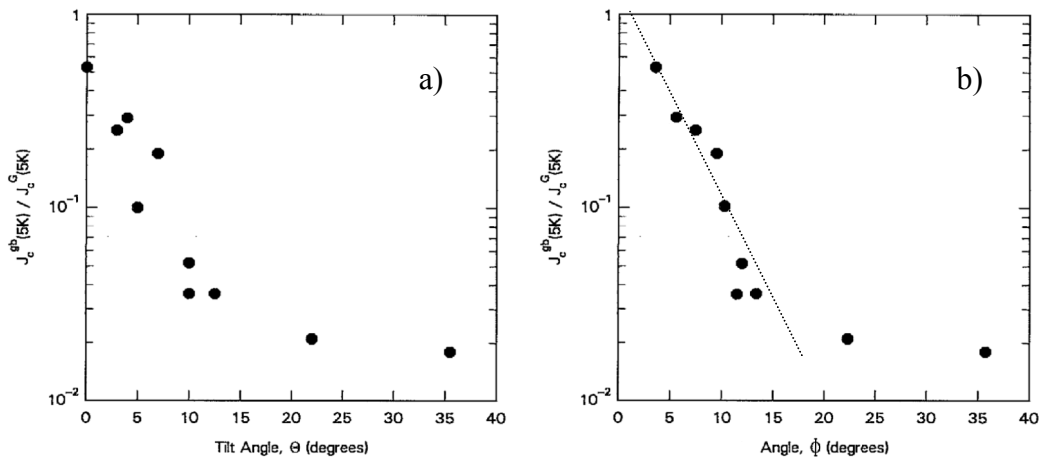


Figure 1.13 The ratio of intra-grain to inter-grain critical current as a function of bicrystal angle a) in the a-b plane and b) in 3 directions. Adapted from ref. [42]

Other experiments were carried out to examine the effects of different grain boundary misorientation components [42]. Most boundaries studied still had more than one misorientation component but the major component is indicated by the symbol in figure 1.14. The most significant result of this series of experiments is that the type of boundary does not

make much difference to the effect on the critical current – only the absolute value of the misorientation angle determines j_c .

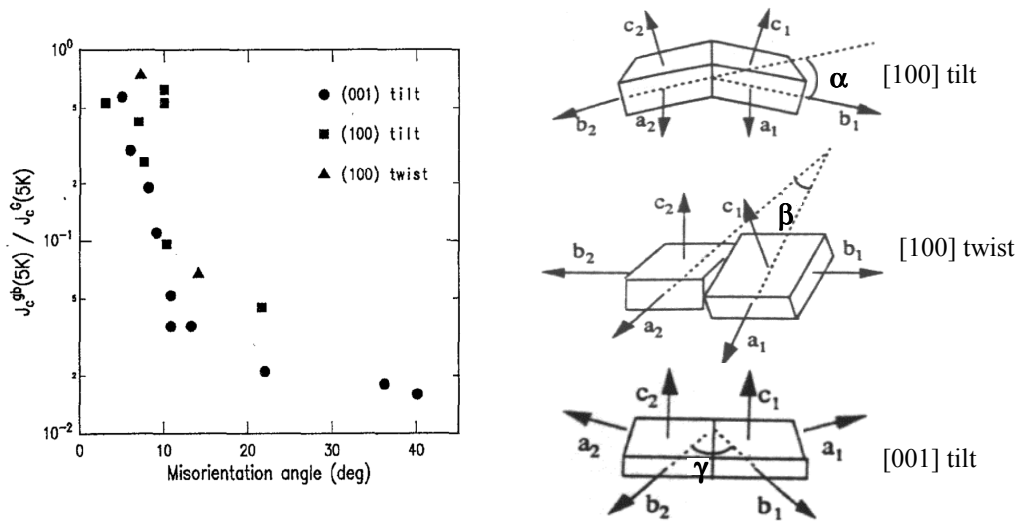


Figure 1.14 Bicrystal data for different boundary types [42]

An important step towards determining more accurately a quantitative relationship between j_c and θ was made by the experiments of Ivanov et al. [43] who obtained a more consistent set of results enabling them to plot the absolute value of the grain boundary j_c against misorientation angle as shown in figure 1.15.

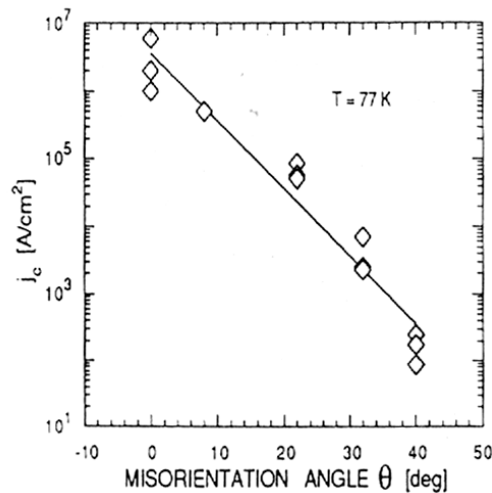


Figure 1.15 The dependence of the grain boundary critical current on misorientation angle for [001] tilt boundaries from [43].

This data indicates that the relationship between j_c and θ is exponential, of the form

$$j_c = j_{c0} \exp\left(-\frac{\theta}{\alpha}\right) \quad (1.16)$$

Several other workers have since found a similar exponential dependence, giving good fits to equation 1.16. The results of Heinig et al. [44] when plotted as the absolute value of the boundary j_c are similar to those of Ivanov et al. and Verebelyi et al. [45]. A collection of all this data [46], along with that for films deposited by LPE and bulk YBCO boundaries [47, 48] is shown in figure 1.16.

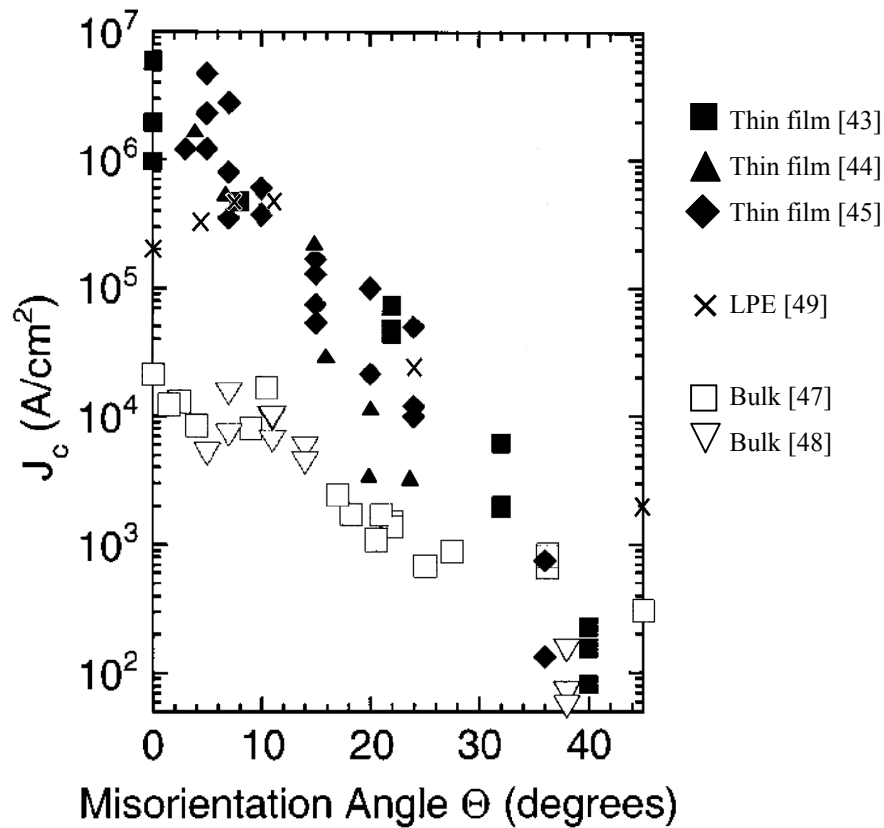


Figure 1.16 J_c vs grain boundary angle data for [001] tilt boundaries in YBCO at 77K. Open symbols represent bulk samples, filled symbols thin films and crosses LPE films. The figure is adapted from [46] and [50].

Table 1.5 A summary of the values of $j_c(0)$ and α fitted to equation 1.16 for measurements on [001] tilt boundaries in thin film and bulk YBCO in self field at 77 K.

Author	Sample type	$j_c(0)$ (MA cm ⁻²)	α (°)
Ivanov [43]	Thin film	3	4.4
Heinig [44]	Thin film	8	3.8
Verebelyi [45]	Thin film	3	3.2
Todt [47]	Bulk	0.03	8.7
Field [48]	Bulk	0.04	6.5

1.6.2 The nature of grain boundaries

The early work of Dimos et al. [41, 42] on YBCO grain boundaries highlighted a significant difference between the behaviour of low angle and high angle grain boundaries. For misorientation angles above 5-10°, the grain boundary behaved as a resistively shunted Josephson junction with weak electromagnetic coupling. Ivanov et al. [43] also observed weak link behaviour for boundaries with angles greater than 22° but not in samples whose misorientations were 8° or less. A characteristic of such weak links is that the critical current density decreases dramatically in small magnetic fields, which will be a significant problem for most potential applications. It should be noted that despite being in the ‘high angle regime’, 22° bicrystal boundaries can be rather strongly coupled [51], which is thought to be due to the fact that the grains on either side of the boundary share a near coincidence site lattice.

Low angle grain boundaries (LAGBs) on the other hand are more strongly coupled and have current-voltage characteristics indicating dissipation by flux flow. In addition to the different electromagnetic properties of low angle grain boundaries from higher angle boundaries, the LAGB also has a very different structure, being composed of an array of edge dislocations as shown in figure 1.17.

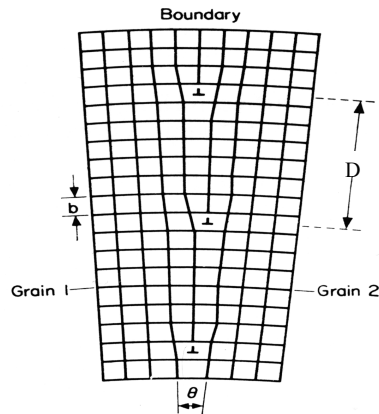


Figure 1.17 An array of edge dislocations from [52]

The dislocation spacing, D is related to the burger's vector, \mathbf{b} , and the grain boundary angle θ by :

$$D = |\mathbf{b}| / 2 \sin(\theta/2) \quad (1.17)$$

In YBCO, the burgers vector is the lattice vector along either the a or b edge of the unit cell and its magnitude is therefore approximately 0.39 nm.

Dimos et al. noted that the dislocation spacing, D , is approximately proportional to $1/\theta$ for small angles, as was the normalised j_c of the boundaries they measured. This led them to suggest the following model for the reduction in j_c based on the presence of dislocations. The superconducting order parameter in the region around a dislocation core is depressed by the structural disorder and distortions arising from the strain field. This region of suppressed superconductivity extends out to some radius, r , around each core and effectively reduces the cross-sectional area of the grain boundary through which the supercurrent may flow. The model does predict that a plateau can occur at high angles as the dislocations cores will overlap when their spacing is less than their diameter. The value of the critical boundary angle, θ_{crit} , at which this occurs is found by substituting $D=2r$ into equation 1.17 giving

$$\theta_{\text{crit}} = \sin^{-1} (|\mathbf{b}|/4r) \quad (1.18)$$

If the core radius is assumed to be equal to the burgers vector, the critical angle is 30° , which is consistent with the Dimos results. There is however some inconsistency at low angles. For a 5° boundary, the dislocation cores (of diameter 0.78 nm) are 4.4 nm apart, shown schematically in figure 1.18. Less than 20% of the boundary area is taken up by the cores and thus one would only expect the j_c of a 5° to be around 20% lower than $j_c(0)$ whereas in fact it is around an order of magnitude smaller. Indeed, the critical current should fall off as $(D-2r)/D$ and, as $\sin \theta \approx \theta$ for small angles, the relationship should be approximately

$$\frac{j_{cb}}{j_{cg}} = 1 - \frac{2r\theta}{|\mathbf{b}|} \quad (1.19)$$

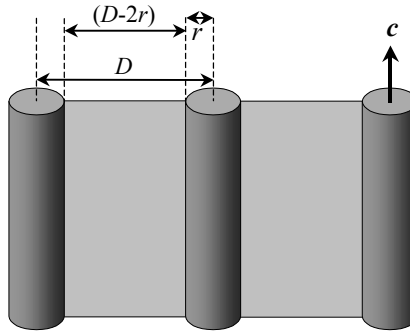


Figure 1.18 Schematic of the dislocation cores for a 5° boundary which have a diameter of 0.78 nm and are 4.4 nm apart (from [38]).

Chisholm & Pennycook [53] showed that a fit to the data of Dimos et al. for boundaries up to 10° indicated an effective core radius which is approximately 3 times greater than the burgers vector. They suggested that the origin of this extended effect of the dislocation could be its associated strain field which would be responsible for reducing the order parameter. This larger core size was confirmed by the observations of Gao et al. who estimated the radius to be approximately 1 nm through TEM [54]. Predictions of the strain fields demonstrated that for angles up to about 10° , a superconducting path between dislocations would remain, but that thereafter, the structural order would be destroyed all along the boundary. A 10° boundary in YBCO has been found to exhibit a crossover between strong and weak coupling behaviour at 75 K by Redwing et al. [55].

Whilst the dislocation model goes some way in describing the approximate form of the low angle relationship and the transition to weak link behaviour at about 10° observed in these early experiments, there are a number of arguments which suggest that the true mechanism may be more complex. Firstly, the strain model only considers the edge dislocations which comprise an [001] tilt boundary. Twist boundaries are composed of networks of screw dislocations and thus have very different strain fields from those surrounding edge dislocations. This would be expected to cause such boundaries to have different electrical properties [56] but measurements have shown that their effect on the critical current is very much the same. In addition, experiments on bulk YBCO bicrystals [57] have shown that in some cases the current remains approximately constant up to boundary angles of around 15° . Also since the early experiments it has become apparent that in fact the high angle plateau region may not exist at all. As indicated earlier, when the absolute value of the boundary j_c is plotted, measurements show an exponential decrease across the entire range of angles.

An aspect of importance to the critical current of the boundary is the symmetry of the order parameter [58] which seems to be based on a $d_{x^2-y^2}$ wavefunction. Due to the anisotropy of HTS materials, the order parameter is expected to be suppressed at any interface between misaligned regions. The effect becomes apparent if a grain boundary is non-planar, being either faceted or meandering. Another factor in the transport of currents across a boundary is the possible variation of stoichiometry, particularly the oxygen content. The model of Moeckly et al. [59] proposes that due to electromigration, there are filaments of well oxygenated superconducting regions sandwiched between regions of normal material.

A recently proposed mechanism for the reduction in grain boundary j_c is electronic band bending, analogous to the effect of boundaries in semiconductors. The band bending is thought to occur due to a cation surplus at the interface and affects the density of mobile charge carriers, another mechanism by which the order parameter can be reduced [60].

1.6.3 Flux pinning at grain boundaries

As LAGBs are composed of arrays of dislocations, they have the potential to act as favourable sites for flux vortex pinning, especially since the size of the dislocation cores is comparable with the coherence length of YBCO in the a-b plane. Heinig et al. [44] determined the irreversibility field, B_{irr} , for grain boundaries up to 20° and found an increase for boundary angles up to 10° and a sharp decrease thereafter. They attribute the increase as being due to pinning by the dislocation cores along the grain boundary and the subsequent decrease as due to the transition to weak link behaviour. Diaz et al. [61] studied the effect of an angular variation in applied field on j_c in a 4° [001] tilt YBCO thin film bicrystal boundary. For fields up to 3 T, a distinct peak in the inter-grain critical current is observed when the field is approximately aligned along the c-axis. The peak is absent for intra-grain measurements, indicating that the dislocation cores do cause an enhanced pinning effect at the boundary. The effect is not seen at higher fields due to the fact that the j_c is limited by the grains, as the irreversibility field is exceeded.

Diaz et al. [39] showed that for a track containing a 4° boundary, practically the entire track voltage is actually generated in a very small region in the vicinity of the boundary. This leads to a field at the boundary around 10^4 times greater than that within a grain. When the vortices at a grain boundary become depinned, the local electric field can be high enough that the flux flow regime is observed. This is confirmed by the observation of linear current-voltage characteristics for inter-grain measurements as shown in figure 1.19.

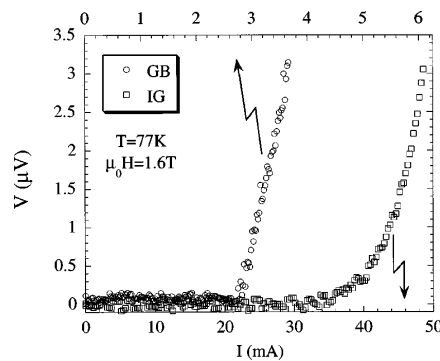


Figure 1.19 Intra-grain and inter-grain V - I characteristics for 4° bicrystal (from [39]).

1.6.4 The effects of grain and boundary on J_c

It is clear that the mechanisms which control the critical currents within the grains and across the boundaries are very different. The intra-grain current is determined by how well defects such as twin boundaries, vacancies and dislocations are able to pin flux vortices. Pinning at the grain boundary may be enhanced by the presence of an array of dislocations which act as good pinning centres, but the critical current will be lowered by a reduction in the effective superconducting area of the boundary and above some critical angle the boundary will act as a weak link.

Because the initial experiments of Dimos et al. produced an inconsistent set of films (in that the intra-grain j_c varied widely), they normalised the boundary j_c to the grain j_c . However, by doing this, they masked a good exponential relationship in their own data (apart from the poor samples whose intra-grain j_c s were low) and other workers have since presented their data in the same way [44, 48]. This has caused a large spread in the published experimental data as demonstrated in figure 1.20.

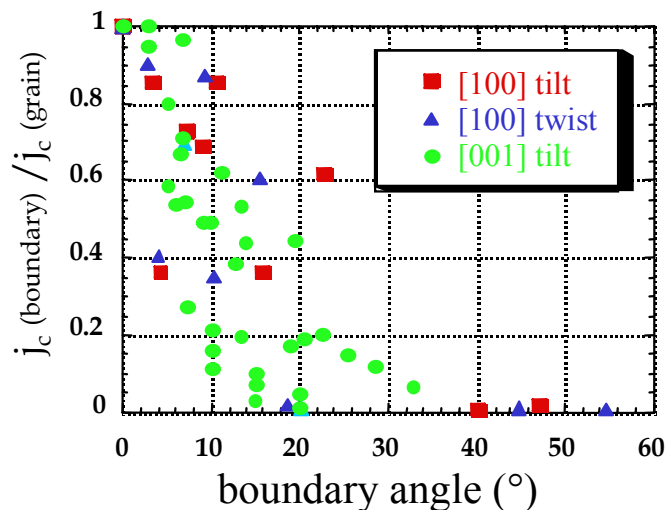


Figure 1.20 Collection of data plotted as j_{cb}/j_{cg} . Adapted from [62].

The j_c of the boundary may actually be higher than that of the grain, especially for very low angle boundaries, where a large area of the boundary retains a high order parameter. Of course this is difficult to measure because in practice one measures the j_c of a boundary in

series with two grains. The existence of a low angle plateau, where the properties of the grain and boundary appear to be equivalent is observed frequently. The first possible explanation is that they really are the same – it has been suggested that twin boundaries, which are prevalent within the grains may have a similar effect on the critical current as 1.8° grain boundaries [63]. Alternatively, the measurements may simply be the same because the properties of the grains determine both the intra-grain and inter-grain measurements of J_c .

Measurements on 2° bicrystal boundaries [64] have recently shown no decrease in j_c for a track measured across the boundary relative to one within the grain. However for a 2.5° boundary, a difference is observed. Similar experiments [65] show that the j_c - T curves for inter-grain and intra-grain tracks in a 2° sample superimpose, but that for a 4.8° sample, the j_c of the boundary is lower. Previously workers have found a crossover between limitation by grains rather than boundaries at higher angles, which suggests lower levels of intra-grain pinning in those samples [66].

Another recent measurement demonstrates that in a RABiTS coated conductor sample, only boundaries which are greater than 4° show evidence of flux penetration in a magneto-optic image [67]. However, it is unlikely that this represents a fundamentally significant threshold in coated conductors, rather it is just the level at which full penetration is attained in one particular coated conductor sample. If the distribution of grain boundary angles were pushed to lower angles, it may well be that 4° , then 3° boundaries would have to become flux flow channels in order to reach full penetration. At some stage, however, one would see a transition point, where the flux would begin to flow through the grains rather than along the boundaries. The situation is complicated somewhat further in coated conductor samples due to the presence of a fine scale mosaic YBCO grain structure, within the larger scale grains which are transferred from the substrate.

1.6.5 The effect of an applied magnetic field

To predict how the j_c vs θ relationship may change in an applied field, we can consider the separate effects on the low and high angle boundaries and the grains. For a modest field

(around 0.1 T), the j_c of the grain and low angle boundaries will decrease by similar amounts. However, there will be a much more significant fall in j_c for grain boundaries which are weak links. A factor of 20 difference between the 10° and 15° boundaries has been measured at low fields.

At higher fields (a few T), another effect becomes significant – the critical current of the grain decreases more rapidly than that of the boundary, as there is less pinning. When the irreversibility field is reached the grain boundary will no longer be the factor that limits j_c . For a 7° boundary measured at 77 K, a crossover to grain-limited J_c was measured by Verebelyi et al. [45] to be around 5 T (and 3 T for a 4.5° boundary). The work of Diaz et al. shows a crossover at around 5 T for 4° boundaries. The difference between these results is probably due to the fact that the degree of pinning in the intra-grain regions tends to vary significantly between samples.

In summary, whilst there is some physical transition between strong and weak link behaviour (at around 10° in YBCO), there is no evidence of a fundamental low angle plateau for grain boundary transport. It is more likely that it is the relative levels of pinning in the grains and at the boundaries which can lead to measurements on inter-grain tracks being determined by the grain rather than the boundary even in low magnetic fields.

1.6.6 Grain boundary doping

A novel method of increasing the critical currents of YBCO grain boundaries has recently been developed. As mentioned in section 1.6.2, an excess of positive charge is responsible for band bending effects near a grain boundary interface lowering the critical current. By replacing some of the Y^{3+} ions with Ca^{2+} , this charge build-up can be reduced and Schmehl et al. [68] and Hammerl et al. [69, 70] have shown that at 4.2 K, the j_c of a 24° boundary is increased by an order of magnitude for $Y_{1-x}Ca_xBa_2Cu_3O_{7-\delta}$ with $x=0.3$. This is demonstrated in figure 1.21. A limitation of this method however is that the Ca doping reduces T_c and thus at 77 K, the effect of doping the boundaries is counteracted [58]. For this reason, it is necessary to selectively overdope the boundaries in order to combine the high T_c of undoped

grains with an improved j_c of doped boundaries. This has been achieved by utilising the higher level of grain boundary diffusion in multilayers [69], and for a doped trilayer, the j_c of a 24° boundary was increased from 5×10^4 to 3×10^5 Acm^{-2} .

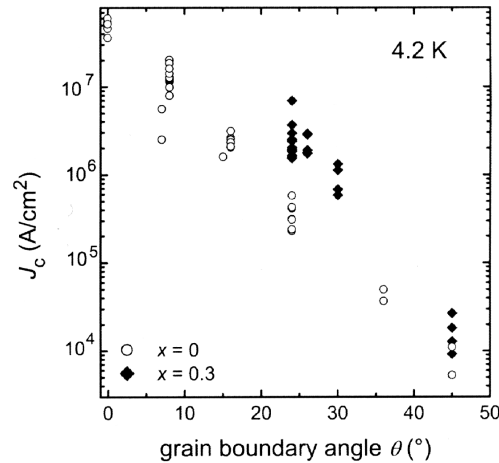


Figure 1.21 Measurements of J_c on doped [001] tilt bicrystal boundaries at 4.2 K adapted from [69]. The undoped sample data (open circles) is from [58].

Importantly, this effect has been reproduced for lower angle grain boundaries, of the type typically found in coated conductors. Daniels et al. [71] have also shown that the critical current in 5° bicrystal boundaries may be increased across a range of magnetic fields at 44 K by doping with 0.3Ca. The performance of these overdoped samples actually becomes grain limited for fields greater than 2 T.

1.6.7 Grain boundaries in other high T_c materials

The description of the behaviour of grain boundaries has so far concentrated on YBCO, as that it is the material on which the majority of work has been focussed. However, a number of measurements have been made for BSCCO and TBCCO. Mayer et al. [72] measured the j_c of [001] tilt BSCCO boundaries to be approximately an order of magnitude lower than those of YBCO at 77 K, a result confirmed by the work of Amrein [73], though at 4.2 K, a smaller difference was observed as shown in figure 1.22.

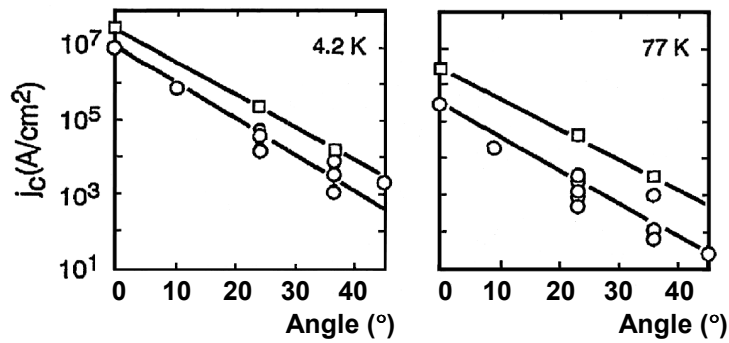


Figure 1.22 Critical current density of [001] tilt BSCCO grain boundaries (circles) in comparison with YBCO (squares) from [73].

It was suggested by Zhu et al. [74] that the [001] twist boundaries of BSCCO are not weak links as they measured a large range of bicrystal angles and found the critical current to be approximately independent of the boundary angle. However the fact that the critical current of the grains in their sample was as low as 500 Acm^{-2} [75] indicates that their result is most likely to be due to the intra-grain regions of the tracks being responsible for determining the measured j_c .

The grain boundary behaviour of TBCCO also appears to show the same qualitative behaviour as YBCO. Sarnelli et al. [76] found a transition from strong to weak link behaviour at around 20° and an exponential reduction of j_c across the angular range. The absolute values of the critical currents appear to be approximately the same as those in BSCCO, though only a small number of experiments have so far been performed.

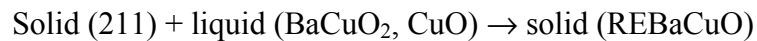
1.6.8 Consequences for 1st generation wires and tapes

Due to the brittle nature of the high T_c oxides, most wires and tapes are composites of the superconductor and a normal metal, which is usually silver. A popular route is the powder in tube (PIT) method in which a silver tube is filled with oxide powder before being drawn to a smaller diameter and sintered at a high temperature (around 900°C). One problem with this method is that it can be difficult to supply sufficient oxygen to the superconductor and so an

alternative route is the metal core composite wire, which has the superconductor coated onto the outside of a metallic core.

In order to produce a wire, individual filaments of the drawn PIT material are placed into another Ag tube. This improves the mechanical properties [77] and leads to a larger interface between the superconductor and Ag, which is desirable for texture development. This tube can then be drawn down in order to produce a multifilamentary wire. Further heat treatment is required in order to improve the texture and heal cracks which form during mechanical deformation. The PIT process has proved very successful for BSCCO materials, as rather good alignment of the plate-like grains is achieved during thermomechanical processing and conductors with critical current densities over 10^4 Acm^{-2} can be produced [77, 78].

One way in which some degree of crystallographic alignment in YBCO may be achieved is through the melt texturing process. If a melt is directionally solidified in the presence of a temperature gradient, the grains align preferentially with the a-b plane parallel to the sample length. In order for the material to be melt textured, it must display a liquidus – peritectic equilibrium in the phase diagram [79]. An example of such a peritectic reaction is



Because the paramagnetic susceptibility of the rare earths is anisotropic, an alternative alignment method is to use a static magnetic field to align crystals which precipitate from a melt. There are two contributing factors to the magnetic forces tending to align such a precipitate, the magnetic moment tending to align the longest dimension parallel to the field and the moment which aligns the axis of largest susceptibility along the field direction for a paramagnetic material. For YBCO, the shape factor is small, and so the c-axis, which has a larger χ , aligns along the direction of the field. Such a technique may be used to produce texture in a bulk sample.

Due to the fact that superconducting materials tend to fracture most easily with an a-b cleavage plane, there is a tendency for powders of some materials, particularly BSCCO, to

form plate-like grains with the c-axis perpendicular to the plate surface. These grains may then be aligned through mechanical processes such as rolling, pressing, extrusion or doctor-blading.